

# Experimental investigation of plasmas in a Q-machine

**Petersen, P.I.**

*Publication date:*
1974

*Document Version*
Publisher's PDF, also known as Version of record

A. E. K. Risø

Risø - M · 1739

Risø - M - 1739

Title and author(s)

# Experimental investigation of plasmas in a Q-machine

by

Peter Ischiel Petersen

Date August 1974

Department or group

Physics

Group's own registration number(s)

43 pages + tables + 24 illustrations

**Abstract**

This report contains some of the results of the work in which I have participated during the past 2 years (1972-1974) in the Q-machine group at Risø.

After a short introduction follows a theoretical discussion on collisionless damping of ion acoustic waves in the case where the derivative of the undisturbed velocity distribution function at the phase velocity equals zero. Then follows a description of the Q-machine and of the preliminary results of the experiments on electron heating. Turbulence in a plasma is treated on the basis of dimensional arguments together with an experiment on turbulence in a cusp Q-device in the next section. In the last section a simple theoretical derivation is given of the Farley instability and a description of the first experimental investigation of this instability in a laboratory.

**Available on request from the Library of the Danish Atomic Energy Commission (Atomenergikommissionens Bibliotek), Risø, Roskilde, Denmark.
Telephone: (08) 35 51 01, ext. 334, telex: 5072.**

Copies to

Abstract to

Fi 25-204

ISBN 87 550 0285 4

CONTENTS

## I. Introduction

Plasma physics is a fairly new branch of natural science. The term "plasma" was introduced by Langmuir in 1929 when describing the properties of matter in gas-discharge tubes. However, only within the last fifteen years serious experimental studies have taken place; stimulated by the hope of producing energy by controlled thermonuclear reactions.

In astrophysics the interest for plasma physics is also increasing. This is a consequence of the fact that more than 99 per cent of the matter in the universe is plasma and that the interplanetary medium nowadays is intensely studied experimentally, by means of cosmic probes.

A great variety of plasma physical phenomena can be studied in a Q-machine. For the past 2 years the work in the Q-machine group at Risø has been concentrated on the propagation of linear ion acoustic perturbations, as well as a few specific problems of geophysical interest.

Most of the results in this report have been obtained during the past 2 years and have been published elsewhere. This concerns the theoretical discussion on collisionless damping of ion acoustic waves in the case where the derivative of the undisturbed velocity distribution function at the phase velocity equals zero (Ref. 11), presented in section II. In section V is presented an experimental investigation of turbulence in a cusp geometry (Ref. 29). In section VI is given a simple theoretical derivation of the Farley instability, based

on the fluid picture, which has not been published before, while the experimental investigation has (Ref. 41).

## II. The Vlasov-equation

There exists a variety of mathematical models for a plasma, each one of which treats certain classes of phenomena correctly and others incorrectly. One model, the Vlasov model is believed to be more useful than any other in describing the dynamical behaviour of most plasmas of interest.

The model consists of one equation, the Vlasov equation, for each component of the plasma. These equations are coupled through the Maxwell equations. The Vlasov equation may be expressed in the form

$$(1)\quad \left\{\frac{\partial}{\partial t} + \underline{v}\cdot\frac{\partial}{\partial \underline{x}} + \frac{e_j}{m_j}\left(\underline{E}(\underline{x},t) + \underline{v}\times\underline{B}(\underline{x},t)\right)\cdot\frac{\partial}{\partial \underline{v}}\right\} f_j(\underline{x},\underline{v},t) = 0$$

where $f_j(\underline{x},\underline{v},t)$ is the one-particle distribution function of the jth plasma component, $e_j$ and $m_j$ are the charge and mass respectively, of the jth component particle. $f_j(\underline{x},\underline{v},t)$ is defined so that $f_j(\underline{x},\underline{v},t)\, d\underline{x}d\underline{v}$ is the number of particles located in a phase-space volume element $d\underline{x}d\underline{v}$ centered at $(\underline{x},\underline{v})$ at time t. The electric and magnetic fields $E(\underline{x},t)$ and $B(x,t)$ are determined self-consistently from the Maxwell equations.

$$(2)\quad \nabla\cdot\underline{E} = \rho/\varepsilon_0$$

$$(3)\quad \nabla\times\underline{E} = -\frac{\partial \underline{B}}{\partial t}$$



$$(4)\quad \nabla\cdot\underline{B} = 0$$

$$(5)\quad c^2(\nabla\times\underline{B}) = \underline{j}/\varepsilon_0 + \frac{\partial \underline{E}}{\partial t}$$

where $\rho$ and $\underline{j}$, the charge and current densities can be written as

$$(6)\quad \rho(\underline{x},t) = \rho_{ext}(\underline{x},t) + \sum_j \int e_j f_j(\underline{x},\underline{v},t)\, d\underline{v}$$

$$(7)\quad \underline{j}(\underline{x},t) = \underline{j}_{ext}(\underline{x},t) + \sum_j e_j \int d\underline{v}\ \underline{v} f_j(\underline{x},\underline{v},t)$$

This set of equations neglects discrete particle interactions and the neutral component of the plasma and quantum mechanical processes. For a fusion plasma these are reasonable approximations since the temperature is so high ($T \sim 10$ keV) that the collision frequencies are rather small ($\nu_{ii} \sim 1\,Hz$, $n_i \sim 10^{17}\,cm^{-3}$)[2] and that the plasma is fully ionized ($n_u/n_i \sim 10^{-14}$ where $n_u$ and $n_i$ are the densities of the neutrals and ions respectively).

The approximations are also reasonable for a low density Q-machine plasma $n \sim 10^8\ cm^{-3}$. Thus a Q-machine is a useful tool for testing the validity of the Vlasov model.

The Vlasov-Maxwell equations (Eq.(1) - (5)) are a nonlinear set of equations and therefore hard to solve even numerically. Therefore, more approximations have to be invoked depending on the problems that have to be solved.

## II. 2. The linearized Vlasov equation

For small longitudinal electrostatic ion perturbations propagating along the magnetic lines of force, the ions can be described by the linearized Vlasov equation

$$\frac{\partial f(x,v,t)}{\partial t} + v \cdot \frac{\partial f(x,v,t)}{\partial x} + \frac{q}{m_i} E(x,t) \frac{\partial f_0(v)}{\partial v} = 0 \tag{8}$$

where $f_0(x,v,t)$ is the zero order ion velocity distribution function and $f(x,v,t)$ is the perturbed ion velocity distribution function, q and $m_i$ are the charge and mass of the ions respectively.

By assuming that the electrons behave as a massless, isothermal fluid and that quasi-neutrality prevails one gets by neglecting the electron inertia ($m_e \ll m_i$) that the electric field (assuming that there is no external imposed electric fields) is given by

$$E(x,t) = - \frac{\varkappa T_e}{q} \frac{1}{n_0} \frac{\partial n(x,t)}{\partial x} \tag{9}$$

where $\varkappa$ is the Boltzmann's constant, and $T_e$ is the electron temperature, $n_0 = \int f_0(v)dv$ and $n = \int f(v)dv$ is the zero order and perturbed densities. By inserting Eq. (9) in Eq. (8) one gets

$$\frac{\partial f(x,v,t)}{\partial t} + v \frac{\partial f(x,v,t)}{\partial x} = c_e^2 \frac{1}{n_0} \frac{\partial n(x,t)}{\partial x} \frac{\partial f_0(v)}{\partial v} \tag{10}$$

where $c_e^2 = \varkappa T_e/m_i$.

Often an equation like Eq. (10) is treated by means of the "Landau first pole" technique[3]. The result of such a procedure is that the damping (Landau damping) of the wave is proportional to the derivative of the equilibrium velocity



distribution function. Several authors[4-11] have argued against the validity of this technique. Hirshfield and Jacob[4] show that "the interpretation of experiments on the spatial Landau damping is complicated by the contribution of the free streaming, initially perturbed particles". The same conclusion is obtained from theoretical as well as experimental investigations among others by Christoffersen et al.[9] in cases where $T_e/T_i \leq 3$.

Christoffersen et al.[9] have solved Eq. (10) by means of the Green's function method for stable distribution functions, that is, functions that have only stable or damped solutions according to the "Landau first pole" technique. For the boundary conditions

$$f(x=0,v,t) = g(v) \exp(-i\omega t) \tag{11}$$

and

$$n(x=0,t) = \int_{-\infty}^{\infty} dv\, g(v) \exp(-i\omega t) = \eta \exp(-i\omega t) \tag{12}$$

it was found that the wave density was

$$n(x,t) = \exp(-i\omega t) \frac{1}{\pi} \int_0^{\infty} \frac{1}{u} \exp\left(i\omega \frac{x}{u}\right) \mathrm{Im}\, N(u)\, du \tag{13}$$

where

$$N(u) = -\left\{\eta + u \cdot \int_{-\infty}^{\infty} \frac{g(v)}{v-u} dv \left[1 - \frac{c_e^2}{n_0} \int_{-\infty}^{\infty} \frac{f_0'(v)}{v-u} dv\right]^{-1}\right\} \tag{14}$$

The integration paths in Eq. (14) run below the pole at $v = u$. Im stands for the imaginary part.

Jensen and Petersen[11] have used Eq. (13) to calculate the phase velocity and the damping of an ion acoustic wave

for case I where

$$g(v) = \eta C_i^{-2} \pi^{-1/2} \exp[-(v-2.5c_i)^2/c_i^2]$$

and

$$f_o(v) = n_o C_i^{-2} \pi^{-1/2} \exp[-(v-2.5c_i)^2/c_i^2]$$

and $T_e = T_i$, where $C_i^2 = \gamma k T_i/m_i$

and for case II where

$$f_o(v) = n_o \{ C_i^{-2} \pi^{-1/2} \exp[-(v-2.5c_i)^2/c_i^2]$$

$$+ 0.0205 (c_i/\sqrt{15})^{-1} \pi^{-1/2} [\exp(-(v-4.05c_i)^2/c_i^2)$$

$$- \exp(-(v-3.55c_i)^2/c_i^2)] \}$$

while g(v) is unchanged. The distribution functions are shown in Fig. 1. In case II the distribution function $f_o(v)$ differs from the first one around $v = v_{phase}$, where the derivative equals zero in case II. The results of the calculations are shown in Fig. 2. It is seen that the phase velocity is only slightly different for the two cases. The curves showing the amplitude of the wave follow each other closely up to $xw/c_i \simeq 60$ (3 wavelenths). From hereon the amplitude for case II increases somewhat. This might be due to constructive interference of the free streaming ions, which has also been seen in the calculations of Estabrook and Alexeff[10]. At a distance of $xw/c_i \simeq 160$ the amplitude starts to decrease again.

The conclusion is that it is not a sufficient condition for an ion acoustic wave in a collisionless plasma to be



undamped that $f'_o(v) = 0$ at $v = v_{phase}$. The damping depends on the gross structure of the velocity distribution function rather than just on its slope.

The case where the velocity distribution is unstable according to the "Landau first pole" technique has been studied among others by Jensen et al.[12]. They have used the linearized ion Vlasov equation, assumed the electrons to be a massless isothermal fluid and used the Poisson equation instead of assuming quasi-neutrality. With a zero-order velocity distribution as

$$f_o(v) = \pi^{-1/2} (2c_i)^{-1} \{ \exp[(v-v_d)/c_i]^2 + \exp[(v+v_d)/c_i]^2 \}$$

with $v_d = 1.5\ c_i$ (such distributions can be made in a Q-machine. See section III.2) and with the initial pulse perturbation having a ion velocity distribution

$$f_o(x,v,t=0) = g(v) \frac{1}{\pi} \frac{\alpha x}{x^2+\alpha^2}$$

they found that for $T_e/T_i$ sufficiently large ($T_e/T_i \simeq 4$) the perturbation will split up in two contributions, of which one is stable and the other unstable. Since the drift velocity of the stable pulse normally is larger than the velocity of the front of the unstable contribution it should be possible experimentally to observe the two contributions separately. To do the experiment in a Q-machine it will be necessary to heat the electrons. This might be done with microwave power at the electron cyclotron frequency (see section III.3).

## III. The Q-machine

Since the following chapters are on experiments performed in the Q-machine at Risø, it might be appropriate at this place to describe the machine.

The Q-machine[13] is essentially different from other plasma devices in the way in which the plasma is created. In most devices the plasma is produced by an electric discharge, which invariably creates disturbances. These disturbances are hard to control and difficult to understand. In the Q-machine the plasma is produced by ionization of neutral Cs atoms on a hot tantalum surface.

A schematic diagram of the Q-machine is shown in Fig. 3. The tantalum plate is heated to 2200 K by bombardment of electrons from a filament. From the Cs oven, which contains a mixture of CsCl and Ca, a beam of Cs vapour will be directed towards the hot plate, when the oven is heated to $\sim 300^{\circ}$ C. Since the work function of tantalum ($\sim 4.2$ V) is larger than the ionization potential of Cs ($\sim 3.9$ V), a large fraction of Cs atoms will be ionized when they impinge on the hot tantalum plate, which is also hot enough to emit electrons (the Richardson emission) in sufficient quantities to ensure charge neutrality. A thin sheath, whose properties will depend on the balance between ions and electrons, will form on the plate. The plasma is confined radially by homogeneous magnetic field and is terminated on a surface, which can either be hot or cold. The vacuum



vessel is made of nonmagnetic stainless steel. With glycol as coolant, the temperature of the vacuum chamber wall is held at $-15^{\circ}$ C while the tantalum plates are hot, whereby the background pressure of the neutral Cs is kept very low ($\sim 10^{-7}$ torr). The diameter of the plasma column is determined by the size of the tantalum plate, which has a diameter of 3 cm. The length of the column can at a maximum be 120 cm. The magnetic field strength can be varied continuously up to $\sim 10$ kgauss and varies normally not more than 5% over the length of the machine.

The plasma produced in a Q-machine is very quiescent (hereof the name). The density fluctuation can be less than 5%. The density can be varied in the range $10^{7}$ cm$^{-3}$ to $10^{12}$ cm$^{-3}$. The temperature of the ions and electrons are of the same order as the hot plate, i.e. $\frac{1}{40} T_i \cong \frac{1}{40} T_e \cong 0.2$ eV.

## III. 2. Diagnostic tools

One of the first and simplest methods used in the study of parameters and properties of a plasma was to immerse a small electric probe in the plasma. Densities and temperatures can be deduced by correctly interpreting the current potential characteristic of such a probe.

Although the Langmuir probe (as these probes are called) is very easy to use, it is normally hard to interprete the measurements since the probe in our case will be coated with neutral cesium, which change the work function for the probe

material. This problem can be avoided by heating the probe to $\sim 1000^{\circ}$ C either by having a dc current through the probe or by irradiating it with light from a laser.

In some experiments as for example that of Christoffersen et al.[9] and in an experiment in which one wants to check the theory of Jensen et al.[12] on ion beam instability, it is essential to know the ion velocity distribution function. The distribution function can be obtained by use of an ion energy analyzer.

The analyzer[15] used at Risø is shown in Fig. 4. It closely reremebles the one described by Buzzi et al.[14]. It consists of a brass housing 38 mm long and 22 mm in diameter. A hole 8 mm in diameter in one end of the housing is covered by a copper mesh, 35 μm thick and with 40,000 25 μm x 25 μm holes per $cm^2$. A collector electrode is placed at a variable distance (up to 1.2 mm) behind the mesh. In order to avoid cesium condensation on the mesh-collector system the analyzer can be heated electrically to about $500^{\circ}$ C by a heating spiral.

In operation the analyzer is placed in the plasma as indicated in Fig. 5. The mesh and the housing is biased negatively (-6 to -10 V) with respect to ground in order to reflect the electrons. The plasma column is thus ended at the analyzer housing. The distribution of the ion energies parallel to the magnetic field lines is determined by measuring the current potential characteristic of the collector



plate. If we assume that the analyzer resolution function is very narrow, the ion current to the collector plate as a function of the collector potential $\varphi_a$, is given by

$$I(\varphi_a) = enA\int_{v_{min.}}^{\infty} v f(v)\, dv \qquad (15)$$

where A is the effective mesh area, n is the ion density, and f(v) is the ion velocity distribution function. The minimum velocity, $v_{min.}$, accepted by the collector is given by $\frac{1}{2} m v_{min.}^2 = e(\varphi_a - \varphi_{pl})$, $\varphi_{pl}$ being the plasma potential and m the ion mass. By differentiation of Eq. (15) with respect to $\varphi_a$ one gets

$$\frac{dI(\varphi_a)}{d\varphi_a} \begin{cases} \propto f\left[v = \left(\frac{2e(\varphi_a - \varphi_{pl})}{m}\right)^{1/2}\right] & \text{for } \varphi_a \geq \varphi_{pl} \\ 0 & \text{for } \varphi_a < \varphi_{pl} \end{cases}$$

Thus one gets the velocity distribution function by differentiation of the collector current potential characteristic with respect to $\varphi_a$. This differentiation is obtained by means of the electrical circuit shown schematically in Fig. 5, and the velocity distribution can be displayed on a scope as shown in Fig. 7. The plasma potential is measured in the following way. A cloud of neutral Cs atoms is obtained in the copper tube by heating oven B, Fig. 6. When the ions pass the cloud, some of them will undergo charge exchange and leave cold ions (tube temperature $\sim 500^{\circ}$ K) behind. These ions are formed at the plasma potential and will show up as a small peak centered around the plasma potential (see Fig. 7). The resolution of the analyzer is $\sim 0.03$ eV. The charge exchange process can also be used to make double peak velocity

distributions.

III. 3. Electron heating

In order for a plasma to show strong collective interactions a high electron ion temperature ratio $T_e/T_i$ is necessary[9]. In a Q-machine operated in the normal mode this ratio will be close to 1. It will therefore be necessary to heat the electrons in order to investigate collective interactions in a Q-machine plasma.

Several methods to heat the electrons have been tried in the Q-machine. Christoffersen and Prahm[16] inserted in the plasma a grid, which they connected to an r.f. (1-50 MHz) frequency generator with a power of the order of 100 mW. The grid was kept d.c. floating, while the a.c.-voltage (peak to peak) was varied from 0.5 - 5.0 Volts. The temperature was measured with a Langmuir probe, which was heated electrically to 900° C, and also determined from

$$\frac{T_{e,\text{heated}}}{T_{e,\text{unheated}}} = 2\left(\frac{v_{ph,\text{heated}} - v_d}{v_{ph,\text{unheated}} - v_d}\right)^2 - 1$$

It was found that the electrons could be heated a factor of ~ 5. When the electrons were heated, it was not possible to measure the ion velocity distribution function, and thereby the ion temperature $T_i$, since the analyzer grid had to be biased more negatively than usual (down to -12 V) to repel the electrons. This low repelling voltage causes a low energy resolution of the analyser especially in the



low-energy range. Thus it is only possible to measure an unchanged ion energy distribution function for small increased $T_e$ values ≈ 0.5 eV, but the distribution was believed to be unaffected by the heating voltage, since the heating frequency was higher than the ion plasma frequency. The noise level of the plasma was increased somewhat, when the electrons were heated.

Another method for heating the electrons is to use micro-wave power[17] at the electron cyclotron frequency. The experimental set up is shown schematically in Fig. 8. The Q-machine was operated single ended and the plasma column was terminated by the energy analyzer. The plasma density was of the order $10^9$ cm$^{-3}$, and the temperature of the hot plate was 2200 K. At a magnetic field strength of about 0.4 T, the electron cyclotron frequency is ~ 10 GHz, i.e. in the X-band.

The micro-wave power was fed into the plasma through 1) a micro-wave horn, 2) a resonator consisting of a tube with the axis parallel to the B-field and covered at the ends with grids in order to allow the plasma to flow freely through the tube. The micro-wave power could be varied within a range of 50-250 mW.

Since the resonance is very sharp, a gradient in the B-field was introduced in order to make it easier to find the resonance. The gradient in the B-field has the further advantage that it causes a conversion of the high perpen-

dicular velocity, which is caused by the "heating", into parallel velocity, even though this effect is small since only a small gradient in the B-field is obtainable. An anisotropic distribution as the one the "heating" will cause, is known to be unstable[18] and this instability may cause a Maxwellization of the electrons.

In the experiment the klystron frequency was adjusted to about 10-12 GHz and then the B-field was varied until resonance was obtained. The resonance was accompanied by an increase in the density by a factor of 1.5-2, this is believed to be due to ionization of neutral Cs.

In Fig. 9 is shown measurements of the ion distribution function with and without micro-wave heating. The ions were at the same time cooled by charge exchange during these measurements. The ion distribution is slightly distorted by the electrons owing to ionization of neutral Cs and second ionization of $Cs^+$.

We found that it was possible to heat the electrons by a factor $\sim 2$ by using the resonator. When a conventional micro-wave horn was used the heating was less effective, and the noise level was somewhat higher. We believe that by using micro-wave equipment with a higher power output together with the charge exchange cooling, it will be possible to reach the necessary temperature ratio $T_e/T_i \cong 4$ to investigate collective phenomena in a Q-machine plasma.



A third method of heating the electrons has been tried. In this method a coarse mesh grid was inserted in the plasma 1 cm from the hot plate. The grid was biased to 50-180 V above the plasma potential and the current extracted from the plasma was of the order of $\sim$ 250 mA. The electron temperature, measured with a Langmuir probe, could be increased by a factor 2-3. At the same time the plasma density was increased by a factor of 2-3.

The heating by this method was accompanied by a considerable increase in the noise level and a severe distortion of the ion distribution function.

The mechanism for this heating is not known, but a possible explanation is that a two-stream electron instability is excited between the hot plate and the grid. Nonlinear decay of the unstable electron oscillations then causes the heating of the electrons.

This heating method is not as usable as the micro-wave heating because of considerable increase in the noise level.

## IV. Turbulence

A plasma is a system with a very large number of degrees of freedom. Thus a large number of different kinds of plasma waves with different frequencies and wavenumbers can exist in a plasma. The state of a plasma in which waves of one or of several modes are excited in a wide range of frequencies and wavenumbers is called plasma turbulence.

The determination of the spectrum of plasma turbulence is a central problem in nonlinear plasma theory. A number of theories of plasma turbulence have been formulated[19,20,21], all of which predict a power law spectrum for the amplitude of electrostatic potential fluctuations $\varphi$ of the form

(16) $$\varphi = \varphi_0 k^{-\nu}$$

For low-$\beta$ ( $\beta = 2\mu_0 p/B^2$ is the ratio between the plasma and magnetic pressure) plasma turbulence F.F. Chen[19] predicts on dimensional grounds for the case of drift wave excited turbulence in a nonuniform plasma that the energy spectrum E(k) should vary as $k^{-5}$.

Let us consider the case in which the turbulence is excited by ion sound waves. We[22] are here going to use the same kind of dimensional arguments as F.F. Chen. The spectrum of fluctuations $\tilde{\varphi}$ in plasma potential is defined as

$$\langle \tilde{\varphi}^2 \rangle = \int_0^\infty E(k) k^2 \, dk$$

for the isotropic case. Since $\varphi$ has the dimension $ML^2/eT^2$ (M mass, L length, e charge and T time), E(k) has the dimension $(M/e)^2$ $(L^7/T^4)$. For ion sound waves we have the following characteristic parameter: $c_s$ the sound speed, $m_i$ the ion mass, e the charge and R the linear size of the system. Therefore

$$E(k) \propto (m_i/e)^2 c_s^4 R^3 \Phi(kR)$$

where $\Phi$ is a universal function of its argument. If there



is a region in k-space in which E(k) is independent of R then $\Phi(kR) = (kR)^{-3}$ i.e.

(17) $$E(k) \propto k^{-3}$$

The frequency and the wavenumber spectrum is related through

(18) $$E(\omega)\, d\omega = E(k) k^2 \, dk$$

From the relations (17) and (18) together with the fact that for low frequency ion acoustic waves $\omega = kc_s$ one finds that

$$E(\omega) \propto \omega^{-1}$$

In experiments[19,23-25], in which Langmuir probes have been used to measure the fluctuation in ion saturation current or floating potential, it is necessary to use the assumption that the frequency $\omega$ and wavenumbers k of the fluctuations are related by a constant factor

$$\omega \propto k$$

(also in cases where the turbulence is not excited by ion acoustic waves) since the theories are expressed in k-space, but the experimental equipment required to perform the measurements renders it expedient to measure the fluctuations in $\omega$ space.

In more laborious experiments[26,27] laser scattering technique was used to directly obtain the wavenumber spectrum for ion acoustic turbulence. In both experiments a $k^{-3}$ wavenumber spectrum was found in agreement with the predictions of Kadomtsev[20] and the dimensional arguments

given above.

An interesting question, which is not pertinent for the dimensional arguments used above, but for the more sophisticated theories, is the correct direction of the net energy cascade in a turbulent spectrum. Some investigators[28] maintain that plasma turbulence is analogous to conventional hydrodynamic turbulence, in that the turbulent energy is transferred from low wavenumbers to higher wavenumbers. Others[21] hold that in a plasma there exists, because of the presence of charged particles and due to the electromagnetic nature of plasma oscillations, the possibility of interactions and energy exchange between the turbulent motion and the particles. In such processes the particles can gain energy and are heated. Thus the particle entropy increases and to compensate this increase the phase volume occupied by the waves can decrease. The turbulent energy can thus be transformed from higher to lower wavenumbers.

An experimental investigation of the direction of energy flow is based on the following argument: If there exists a broad peak on the turbulent spectrum that couple energy from an external source to the turbulent spectrum, then one might expect to observe one of the two situations illustrated in Fig. 10. The turbulent spectrum is assumed to obey the power-law relation given by Eq. 16. Fig. 10(a)



shows the situation in which the energy is fed in at a given frequency and energy flows towards higher frequencies. In Fig. 10(b) is shown the situation in which the energy cascades downward towards lower frequencies.

Several cases studied by J.R. Roth[25] showed clearly that the energy was cascading to higher frequencies.

## IV. 2. Turbulence in a cusp geometry

Turbulence spectra have been measured in a cusp Q-machine at Risø[29]. The hot plates were spaced 50 cm apart and the normal magnetic field configuration was modified in order to obtain a magnetic cusp-like geometry with "point" cusps at the two cathodes and a "ring" cusp at the midplane of the device. The magnetic field strength at the cathodes could be varied between 1000 gauss and 2500 gauss. In Fig. 11 is shown the magnetic field strength distribution measured with a Hall probe along the axis of the device. The plasma density in a region, less than 10 cm fra the midplane of the cusp, where the measurements were performed, was typically of the order of $10^{10}$ $cm^{-3}$, while near the hot plates it was about an order of magnitude higher. Radial density profiles measured in the region close to the midplane showed a very smooth plasma density distribution with an e-folding length perpendicular to B of about 10 cm. Close to the hot plate the radial density profiles were as in a normal Q-machine with a uniform magnetic field of a few

thousand gauss. The neutral background pressure was typically 1-2 x $10^{-5}$ mm Hg.

As well the plasma density fluctuations $\tilde{n}$ as the potential fluctuations $\tilde{\varphi}$ were measured with a Langmuir probe made of a tungsten wire 0.2 mm in diameter and with a glass tube shielding so only 0.2 mm of the tip was exposed to the plasma. The signal from the probe was fed through a voltage follower with an input impedance of 1 MΩ, to a Hewlett-Packard spectrum analyzer. A typical power spectrum taken ~ 3 cm from the midplane is shown in Fig. 12. The spectrum shows a nearly $1/f^3$ frequency dependence. Spectra measured close to the hot plates on the other hand showed a $1/f^5$ frequency dependence, which is characteristic for drift wave excited turbulence. It was also found that $\tilde{n}/n \approx e\tilde{\varphi}/\varkappa T$, as expected for electrostatic fluctuations.

To obtain a better understanding of the $1/f^3$ power spectrum near the midplane a double probe as shown in Fig. 13 was used. The double probe consists of two tantalum discs separated by a mylar disc. The probe could be moved across the plasma at a distance of 3-5 cm from the midplane. Two positions of the probe are indicated as "top" and "bottom" in Fig. 13. The $\hat{r} \times \underline{B}$ direction are indicated by the arrow. In both positions the signal from the side facing $\hat{r} \times \underline{B}$ showed a ~30% higher signal than the other side. The difference can evidently not arise from different effective areas of the two sides of the probe. This measurement clearly



indicates an anisotropy in the turbulence, and that there is a "preferred" direction, which coincides with the $\hat{r} \times \underline{B}$ direction.

To further test this point a fork probe as shown in Fig. 14 was used. The fork probe consists of two separate Langmuir probes, which are mechanically connected. Each probe has a tungsten tip 0.5 mm in diameter and an exposed length of 0.8 mm. The tips are 2 cm apart. The fork probe was nearly at the same location (1 and 2 in Fig. 14) as the double probe ("top" and "bottom" in Fig. 13), and positioned in such a way that the plane determined by the probe legs was perpendicular to the axis of the Q-machine. The signals from the two tips filtered through a band pass filter (10 kHz - ~ 100 kHz) were fed to a cross-correlator. A typical cross-correlogram is shown in Fig. 15 for the fork probe in position 1 and "a delayed". The cross-correlation clearly shows a shift $\tau$ of 5 μsec., corresponding to an azimuthal phase velocity $v_{ph}$ of ~ $10^5$ cm/sec. in the $\hat{r} \times \underline{B}$-direction. The same correlogram was obtained for the fork probe in position 2 and "b delayed". The time shift $\tau$ varied proportionally with the field strength. The measured ratio $B/\tau$ is shown in Fig. 16. These data show that $v_{ph}$ varied proportionally to 1/B.

## IV. 3. Discussion of experimental results

The turbulence is believed to be excited by the cen-

trifugal instability[30]. If a fully ionized column with cylindrical symmetry is made to rotate because of a radial electric field, the centrifugal force which results from the rotation can produce what essentially amounts to a Rayleigh-Taylor instability[31].

A radial electric field in a Q-machine is created and determined by the balance of electron fluxes into and out of the hot plates[30]. The magnitude of the radial electric field $E_r \simeq \frac{\kappa T}{e \Lambda}$, where $\Lambda$ is the e-folding length of the radial density profile, is in our case $\sim 0.5$ V/cm at the hot plate. The B-field lines are assumed to be DC-wise equipotential, so that the E-field is "mapped" out to the neighbourhood of the cusp midplane. Here the ions and electrons experience a $\underline{E} \times \underline{B}$ drift with the velocity $v_{\underline{E}\times\underline{B}} \simeq 10^5$ cm/sec.

The phase velocity for this type of waves is for low densities where $k_\parallel \simeq 0$ ($k_\parallel$ is the component of the propagation vector parallel to the B-field) given by the following relation

$$v_{ph} = v_{\underline{E}\times\underline{B}} + v_{i,d}$$

while for higher densities where the electron-ion collisions allow $k_\parallel$ to be large enough that the "drift" mode is excited and then

$$v_{ph} = v_{\underline{E}\times\underline{B}} + v_{e,d}$$



where $v_{i,d}$ and $v_{e,d}$ are the ion and electron diamagnetic velocity, respectively.

In our case where the e-folding length of the density profile $\Lambda \simeq 10$ cm a few centimeters from the midplane gives a $| v_{i,e\,d} | \simeq 2\times10^4$ cm/sec., which is considerably less than $v_{ExB}$. We were thus not able to determine whether the wave was travelling at $v_{ph} = v_{\underline{E}\times\underline{B}} + v_{i,d}$ or $v_{ph} = v_{\underline{E}\times\underline{B}} + v_{i,d}$. The measured phase velocity fits, however, very well with the calculated $v_{\underline{E}\times\underline{B}} \simeq 10^5$ cm/sec. and fits with the 1/B dependence of the $v_{\underline{E}\times\underline{B}}$ drift velocity. The $v_{\underline{E}\times\underline{B}}$ velocity is in the same direction as the measured $\hat{r} \times \underline{B}$ direction.

The most interesting result of the experiment is probably the measured gradual change of the spectrum from an $1/f^3$ frequency dependence near the midplane to $1/f^5$ near the hot plate. The dimensional arguments used by Chen[19] in deriving the $1/k^5$ wave spectrum apply only for wavelength in the range $L > \lambda > \rho_i$, where L is the linear size of the plasma and $\rho_i$ is the ion gyroradius. Close to the midplane the measured phase velocity is $v_{ph} \simeq 10^5$ cm/sec. and a frequency of $f \simeq 150$ KHz (see Fig. 12) corresponds to a wavelength $\lambda \simeq 0.7$ cm, which is much smaller than the ion gyroradius $\rho_i \simeq 5$ cm ($B \simeq 150$ gauss). For wavelengths smaller than the ion gyroradius the ion dynamics should no longer be much affected by the $\underline{B}$-field and the wave motion should begin resembling ion acoustic motion, which as shown has a

flatter spectrum.

Close to the hot plate the wavelength is in the range for which Chen's[19] dimensional arguments are valid and here the $1/f^5$ spectrum is measured in agreement with the theory.

## V. The fluid picture

In the next section is given a simple derivation of the Farley instability based on the fluid picture. In the fluid picture the ions and electrons are considered as conducting fluids, which are described by the continuity equations and momentum equations

$$\partial n_j/\partial t + \nabla \cdot (n_j \underline{v}_j) = 0$$

$$n_j m_j \left( \partial \underline{v}_j/\partial t + (\underline{v}_j \cdot \nabla)\underline{v}_j \right) = -\nabla n_j \times T_j + n_j q_j (\underline{E} + \underline{v}_j \times \underline{B})$$

which can be obtained by taking moments of the Vlasov equation and assuming the pressure to be isotropic.



## VI. The Farley instability

The tidal motion of the earth's atmosphere[32], in conjunction with the geomagnetic field, generates electric fields (the dynamo fields) in the ionosphere, and these fields would, in turn, drive the plasma to move in the direction of $\underline{E}\times\underline{B}$. At an altitude of 90÷120 km the electrons drift freely but the motion of ions is strongly impeded by collisions with neutral particles, because the relations between the collision frequency $\nu_n$ and gyrofrequency $\Omega$ are such that $\nu_{en} \ll \Omega_e$ and $\nu_{in} \gtrsim \Omega_i$. This results in an electron current flowing in the ionosphere. If the electron drift velocity relative to the ion background exceeds the local sound speed ($\sim$ 360 m/sec), longitudinal plasma waves will grow[33,34]. This two-stream instability is generally held responsible for the so-called type I irregularities in the equatorial electrojet. These are, in addition with other irregularities, called by Balsley[35] type II irregularities, observed in a series of radar experiments[36] at Jicamarca, near the geomagnetic equator. The type II irregularities are apparently associated with a density gradient drift instability[34,36-40].

Rogister and D'Angelo[34] have presented a unified treatment of the two instabilities, based on a fluid treatment for both ions and electrons, with suitable collision term, while Farley[33] has used the Vlasov equation with the BGK collision term

(19) $$\frac{\partial f_j}{\partial t} + \underline{v}\cdot\frac{\partial f_j}{\partial \underline{x}} + \frac{e_j}{m_j}\left[\underline{E} + \underline{v}\times\underline{B}\right]\cdot\frac{\partial f_j}{\partial \underline{v}} = -\nu_j\left[f_j - \frac{N_j}{N_o} f_{oj}\right]$$

and Poisson's equation to obtain the dispersion relation, which then is solved numerically. Thus Farley was able to explain the type I instability.

VI.2. The theory

In this report I will derive the Farley instability (type I) from a fluid picture in a more simple way than that of Rogister and D'Angelo.

In the framework of a two-fluid theory, where we take into account collisions with a neutral background the equations to be considered are the following:

(20) $$\partial n_j/\partial t + \nabla\cdot(n_j \underline{v}_j) = 0$$

(21) $$n_j m_j\left(\partial \underline{v}_j/\partial t + (\underline{v}_j\cdot\nabla)\underline{v}_j\right) = -\nabla n_j \varkappa T_j - n_j q_j(\underline{E} + \underline{v}\times\underline{B}) - \nu_j n_j m_j \underline{v}_j$$

where $m_j$ and $q_j$ are the mass and charge of the j-component particle, while $n_j$ is the particle density, $\underline{v}_j$ the fluid velocity, $T_j$ the temperature of the j-component fluid, and $\nu_j$ is the collision frequency between j-component particles and neutrals, $\varkappa$ is the Boltzmann constant. Further we assume the plasma to be uniform, that there is quasi-neutrality ($n_e \simeq n_i$), that $T_e = T_i$, and that the $\underline{E}$-field is in the x-direction and $\underline{B}$-field is in the z-direction.

The zero-order solution for the electrons is (since $\Omega_e \gg \nu_e$)



(22) $$v_{oye} = -\frac{\Omega_e^2}{\Omega_e^2+\nu_e^2}\frac{E}{B} \simeq -\frac{E}{B}$$

(23) $$v_{oxe} = -\frac{\Omega_e \nu_e}{\Omega_e^2+\nu_e^2}\frac{E}{B} \simeq 0$$

and for the ions

(24) $$v_{oyi} = -\frac{\Omega_i^2}{\Omega_i^2+\nu_i^2}\frac{E}{B}$$

(25) $$v_{oxi} = +\frac{\Omega_i \nu_i}{\Omega_i^2+\nu_i^2}\frac{E}{B}$$

We assume the first-order perturbations to be travelling waves of the form exp(iky-iwt) where w is complex. By linearizing the equations (2)-(3) and neglecting the electron inertia we get

$$(-i\omega + ikv_{oe})\frac{n_1}{n_o} + ikv_{e1y} = 0$$

$$-ik\varkappa T_e\frac{n_1}{n_o} + eBv_{e1x} - \nu_e m_e v_{e1y} + ike\varphi_1 = 0$$

$$-\nu_e m_e v_{e1x} - eBv_{e1y} = 0$$

$$(-i\omega + ikv_{oiy})\frac{n_1}{n_o} + ikv_{i1y} = 0$$

$$ik\varkappa T_i\frac{n_1}{n_o} + ike\varphi_1 + eBv_{i1x} + (-i\omega + ikv_{oiy} + \nu_i)m_i v_{i1y} = 0$$

$$(-i\omega + ikv_{oiy} + \nu)m_i v_{i1x} - eBv_{i1y} = 0$$

This set of equations has a non-trivial solution, when the determinant

$$\begin{vmatrix} (-i\omega + ikv_{oe}) & ik & 0 & 0 & 0 & 0 \\ -ikxT_e & -\nu_e m_e & eB & ike & 0 & 0 \\ 0 & -eB & -\nu_e m_e & 0 & 0 & 0 \\ ikxT_i & 0 & 0 & +ike & +m_i(-i\omega+ikv_{oi}+\nu_i) & eB \\ (-i\omega + ikv_{oi}) & 0 & 0 & 0 & ik & 0 \\ 0 & 0 & 0 & 0 & -eB/m_i & (-i\omega+ikv_{oi}+\nu_i) \end{vmatrix}$$

is equal to zero. We then find the following dispersion equation

$$(-i\omega + ikv_{oi}+\nu_i)[i\nu_e(\omega - kv_{oi})(i\omega - ikv_{oi} - \nu_i)$$
$$+ (-i\omega + ikv_{oe})\Omega_e\Omega_i + k^2c_s^2\nu_e] + (-i\omega + ikv_{oi})\nu_e\Omega_i^2 = 0$$

where $c_s = \varkappa(T_e+T_i)/m_i$ and $\Omega_j = \frac{eB}{m_j}$. By setting $\omega = \omega_k + i\gamma_k$ with both $\omega_k$ and $\gamma_k$ real, and considering only the case where

$$|\gamma_k| \ll |\omega_k|$$

and
$$(v_{oe} - v_{oi})^2 \gg \frac{\nu_e\nu_i}{\Omega_e\Omega_i} c_s^2 \qquad (26)$$

we find that

$$\omega_k = \frac{kv_{oe}}{(1+2\psi)} + \frac{2\psi kv_{oi}}{(1+2\psi)} + \frac{\psi k^2c_s^2}{(kv_{oe} - kv_{oi})}$$

$$\simeq kv_{oe}\,; \quad \psi = \frac{\nu_e\nu_i}{\Omega_e\Omega_i} \ll 1$$

or

$$\omega_k = kv_{oi} - \frac{\psi k^2c_s^2}{(kv_{oe} - kv_{oi})} \simeq kv_{oi}$$

for $\omega_k = kv_{oe}$ we find

$$(27)\quad \gamma_k = \frac{\nu_e}{\Omega_e\Omega_i}\left[\{(\omega_k - kv_{oi})^2 - k^2c_s^2\} - \frac{\Omega_i^2(\omega_k - kv_{oi})^2}{(\omega_k - kv_{oi})^2 + \nu_i^2}\right]$$

and for $\omega_k = kv_{oi}$

$$\gamma_k = -\nu_e\frac{k^2c_s^2}{\Omega_e\Omega_i}$$

We thus see that only the waves with the phase-velocity equal to the electron drift velocity can grow, while waves with the phase velocity equal to the ion drift velocity are always damped.

We are therefore from now on only discussing the waves with the phase velocity equal to the electron drift velocity.

The growth rate obtained by A. Rogister and N. D'Angelo[34] in the case where there is no density gradient a velocity shear is given by the following expression

$$\gamma_k = \frac{\nu_e}{\Omega_e\Omega_i}\left[(\underline{k}\cdot\underline{v}_{eo} - \underline{k}\cdot\underline{v}_{io})^2 - k_i^2c_s^2\right]$$

This is essentially the same as in Eq. (27) except for the last term in the square bracket in Eq. 27.

For a sufficiently high collision frequency ($\nu_i \gg \Omega_i$) the above derivation does not hold (see Eq. 26). In this case

the ions can be considered as unmagnetized. This case has been considered by Sudan et al.[40] and Rogister and D'Angelo[34]. They found that

$$\omega_k = \frac{\Omega_e \Omega_i}{\nu_e \nu_i + \Omega_e \Omega_i} k v_{oe} \tag{28}$$

and

$$\gamma_k = \frac{\nu_e}{\nu_e \nu_i + \Omega_e \Omega_i} ( \omega_k^2 - k^2 c_s^2 ) \tag{29}$$

From the equations 22-25 and 28,29 it is easily seen for a sufficiently low $\nu_i$ and fixed $\underline{E}$ and $\underline{B}$-field that the instability cannot be excited, since the difference in the drift velocities for the electrons and ions do not exceed the ion sound velocity. When $\nu_i \sim \Omega_i$ it is possible to excite the instability if $E/B > c_s$. For a sufficiently high $\nu_i$ the phase velocity will be lower than $v_{oe}$ (see Eq. 28) and the instability might not be excited even though $v_{oe} > c_s$.

## VI.3. Experimental set-up

So far the only laboratory test[41] of the Farley instability theory has been performed in the Q-machine at Risø.

The Q-machine, which has been described in an earlier section, was operated single-ended with a homogeneous magnetic field. The normal hot tantalum plate was replaced by a double spiral (see Fig. 17) made of a tantalum wire 2 mm in diameter. This spiral was heated to ~2100 K, in order to obtain surface ionization of the neutral $C_s$-beam, by a



current of ~ 100 amp. The outer parts of the spiral were grounded, while the centre was biased to -5.9 V. By using this spiral it was possible to obtain in the plasma column an inward directed radial electric field, which in magnitude increased linearly with radius, such that the $\underline{E}x\underline{B}$ rotation of the plasma was a "solid body" rotation, i.e. shear free. The average electric field strength was ~ 2 V/cm, which as wanted gave an $\underline{E}x\underline{B}$-drift velocity of the same order as the ion sound velocity $c_s$, which in a Q-machine is ~ $4 \times 10^4$ cm/sec, when the B-field is several thousand Gauss.

The reason for using a double spiral instead of a single spiral was that it was not possible with a single spiral to get a sufficiently low voltage drop across the spiral and at the same time have a sufficiently large ionization-surface.

Density and potential measurements were performed by using a set of cylindrical Langmuir probes (effective area ~ $5 \times 10^{-2}$ cm$^2$), which could either be biased to collect the ion saturation current (for density and density fluctuation measurements) or left floating (for potential and potential fluctuation measurements). The background neutral particles were argon atoms and the argon pressure could be varied between ~ $10^{-5}$ mm Hg and ~ $10^{-1}$ mm Hg.

## VI.4. Experimental results

The floating potential was measured across the plasma

column and the result is shown in Fig. 18 for a background pressure $p \sim 1 \times 10^{-5}$ mm Hg. The circles represent the experimental point and the full line is a parabolic fit $V(x) = ax^2 + b$, where x is the distance from the centre of the column. a is found to be 0.61 volt/cm$^2$, and b = -7.4 volt. The -7.4 volt at the centre of the column is consistent with a voltage drop of -1.5 volt in the sheath (see section III) at the spiral which centre was at -5.9 volt. The parabolic fit is seen to be a fairly good one, such that the column can be considered to be shear free.

The plasma was very quiescent at a low neutral background pressure. When the background pressure was increased it stayed quiescent until at a pressure of about $10^{-2}$ mm Hg, where suddenly the noise level increased and distinct modes appeared. The pressure at which onset of the instability was observed, varied with the magnetic field strength. The measured relation is shown in Fig. 19. When the magnetic field was about 7700 Gauss the instability was barely excited and at higher fields it could not be excited at all.

The measured relative density fluctuations $\tilde{n}/n$ are as high as 30-50%, when the clear modes are seen. Measurements of the potential fluctuations, $\tilde{\varphi}$, show that $e\tilde{\varphi} \propto \tilde{n}/n$, as expected for a low $\beta$ -plasma. The profiles of the measured density n and the relative density fluctuations across the column are shown in Fig. 20. The relative density fluctuations are seen to have a minimum at the centre of the column.



The waves excited at a pressure higher than $10^{-2}$ mm Hg was further investigated by means of two Langmuir probes. One of the probes was kept at a fixed position and used as a reference probe, while the other probe could be moved along the column, as well as turned in a plan perpendicular to $\underline{B}$ to describe a full circle with a diameter of 6 cm. In Fig. 21 is shown the measured phase of the oscillation, which had a frequency of 2.5 kHz, as a function of the azimuthal position, $\theta$, of the probe. The magnetic field was 4700 gauss and the background pressure was $3 \times 10^{-2}$ mm Hg. It is seen to be an m = 1 mode; m = 2 and 3 modes were sometimes also seen. The direction of propagation was in all measurements found to coincide with the $\underline{E}\times\underline{B}$ direction. Furthermore, it was found by moving the probe radially, as well as along the $\underline{B}$-field line that there was no measurable change in the phase. This means that $\lambda_\theta \ll \lambda_r$ and $\lambda_\theta \ll \lambda_\parallel$ .

By measurements of the type shown in Fig. 21 the phase velocity was found and its dependence on the magnetic field strength is shown in Fig. 22. The experimental points (the dots) are seen to be fairly close to the $v_{\underline{E}\times\underline{B}} = \underline{E}\times\underline{B}/B^2$ velocity, although somewhat below it. The dotted line is the ion acoustic velocity $c_s = 4 \times 10^4$ cm/sec. In all cases $v_{ph} > c_s$ as expected.

The phase velocity was also measured as a function of the neutral background pressure (see Fig. 23). It is seen that phase velocity decreases with increasing background

pressure.

VI.5. Discussion of the experimental results

The experiment clearly shows that the instability gives rises to waves, which propagate in the $\underline{E}x\underline{B}$-direction and have wavelengths parallel with the $\underline{B}$-field much larger than the azimuthal wavelength.

The measured phase velocity is close to the expected value $v_{\underline{E}x\underline{B}} = \underline{E}x\underline{B}/B^2$. The discrepance can be explained by a partial short-circuiting of the $\underline{E}$-field by the Pedersen current. This current is due to the radial drift of the ions (see Eq. 25). It is seen that this current has a maximum for $\nu_i = \Omega_i$. This has been verified by actual measurements of the radial electric field as a function of the neutral background pressure.

In Fig. 24 the onset of the instability has been compared with the instability boundary obtained from the theory derived in section VI.2. (full line), and with that of Rogister and D'Angelo (dotted line). The experimental data used are those presented in Fig. 19. In converting the argon pressure to an ion-neutral collision frequency a cross-section $\sigma_n = 2\times10^{-14}\,cm^2$ for $Cs^+$-A has been used[42]. It is seen that there is a good agreement with both theories. Though the slope of the instability boundary obtained from the theory derived in this report gives the best fit to the experimental points.



Only the lower instability boundary was checked, since the "high pressure" regime of the theory could not be explored in the Q-machine. In the "high pressure" regime the $C_s$-A collision free mean path is so short that only a very small fraction of the $C_s$ atoms will reach the ionizing surface.

In the theory and experiment in this report the density gradient has been neglected. The simplest way of incorporating it is given by Morse[43]. Instead of using the actual electric field E a "corrected" electric field $E_c = E+T_i/\Lambda$ is used. $\Lambda$ is the e-folding length of the radial density profile. Since $T_i \sim 0.2$ volt and $\Lambda \sim 4$ cm, the "corrected" electric field $E_c$ differs only very slightly (0.05 volt/cm) from the actual electric field E = 2 volt/cm.

VII. Conclusions

In this report I have decribed the experiments performed in the Q-machine at Risø, during the past 2½ years. The conclusions of the different experiments have been given in the sections describing the experiments. The variety of experiments performed in the Q-machine clearly shows the versatility of this device.

VIII. Acknowledgments

This work has been carried out as part of the requirements for obtaining the degree of lic.scient. at the University

of Copenhagen. The scholarship from the Danish Atomic Energy Commission, which made this study possible, is gratefully acknowledged.

I want to thank all members of the Q-machine group for the great help during my years of studying at Risø.



## IX. FIGURE CAPTIONS

Fig. 1 Shape of the $f_o(v)$ and $g(v)$ functions.

Fig. 2 Density and phase of wave, calculated for the two cases.

Fig. 3 A schematic drawing of the Q-machine.

Fig. 4 A schematic drawing of the ion energy analyzer.

Fig. 5 The experimental set-up for the ion energy analyzer.

Fig. 6 The experimental set-up with the charge-exchange oven.

Fig. 7 Differentiated current potential characteristic with the charge-exchange peak.

Fig. 8 The microwave set-up.

Fig. 9 Ion energy distributions measured with and without the electrons heated.

Fig. 10a Logarithmic plot of expected electrostatic turbulence spectrum for the case in which energy is added to the plasma at a descrete frequency, and then cascades to higher frequencies.

b Logarithmic plot of expected electrostatic turbulence spectrum for the case in which energy is added at a descrete frequency, but cascades to lower frequencies.

Fig. 11 The B-field strength along the cusp-axis.

Fig. 12 A typical power spectrum taken at ~ 3 cm from the mid-plane of the cusp.

Fig. 13a Double probe construction.

b Schematic diagram showing two probe positions and the $r \times \underline{B}$ direction (arrow).

Fig. 14a The "fork" probe shown at two positions in a plane normal to the axis of the device, ~ 3 cm from the midplane.

Fig. 15 Cross-correlogram obtained with the "fork" probe. The base line is indicated by an arrow. The time is 10 μs/large div.

Fig. 16 B/T as a function of the $\underline{B}$-field strength. The delay time, $\tau$, is obtained from figures of the type of Fig. 15. The $\underline{B}$-field is measured at the hot plate position.

Fig. 17a The experimental set-up.

b The double spiral.

Fig. 18 Profile of the floating potential across the plasma column [B = 2500 gauss, p = $8 \times 10^{-3}$ mm Hg]. The circles are experimental points and the full line is a parabolic fit.

Fig. 19 The measured relation between magnetic field strength and the argon pressure at which onset of instability is observed to occur. At ~ 7700 gauss wave excitation become marginal.



Fig. 20 Radial density profile (circles and full line) and relative density fluctuations, $\tilde{n}/n$ (crosses and dotted line). [B = 2500 gauss, p = $2 \times 10^{-2}$ mm Hg].

Fig. 21 Azimuthal variation of the phase of the oscillation (f = 2.5 kHz) [B = 4700 gauss, p = $3 \times 10^{-2}$ mm Hg].

Fig. 22 Measured variation of the azimuthal phase velocity with magnetic field strength (the voltage across the spiral is fixed at 5.9 volt). The full line is the $\underline{E} \times \underline{B}$ drift velocity, computed on the basis of the $\underline{E}$ field strength measured at p ≈ $1 \times 10^{-2}$ mm Hg. The sound speed is indicated by $c_s$.

Fig. 23 Dependence of the oscillation frequency (and, therefore, of the azimuthal phase velocity) on argon pressure [B = 2600 gauss].

Fig. 24 A comparison of the observed $\omega_{ci}$ versus $\nu_i$ region of oscillation onset with the prediction of Rogister and D'Angelo's theory (dotted line) and with the theory derived in this report (full line).

References


1. A.A. Vlasov, J. Phys. (U.S.S.R.) 9, (1945) 25.
2. T. Hesselberg Jensen, O. Kofoed-Hansen, A.H. Sillesen and C.F. Wandel, Risø Report 2 (1958).
3. L. Landau, J. Phys. (U.S.S.R.) 10, (1946) 25.
4. J.L. Hirshfield and J.H. Jacob, Phys. Fluids 11 (1968) 411.
5. H. Weitzner, Phys. Fluids 6 (1963) 1123.
6. H. Weitzner and D. Dobrott, Phys. Fluids 11 (1968) 152.
7. H. Weitzner, Proc. of Symposia in Applied Mathematics, American Mathematical Society 18 (1967) 127.
8. S.A. Andersen et al., Phys. Fluids 14 (1971) 990.
9. G.B. Christoffersen et al., Phys. Fluids
10. K. Estabrook and I. Alexeff. Phys. Rev. Lett. 29 (1972) 573.
11. V.O. Jensen and P.I. Petersen, Phys. Lett. 45A (1973) 293.
12. V.O. Jensen, P. Michelsen and H.C.S. Hsuan, to be publisned in Phys. Fluids (1974).
13. N. Rynn and N. D'Angelo, Rev. Sci. Instr. 31 (1960) 1326.
14. I.M. Buzzi, H.J. Doucet and D. Grezillon in Proceedings of the International Conference on Physics of Quiescent Plasmas, Paris (Ecole Polytechnique, Paris, 1969) Vol.III p. 149.





15. S.A. Andersen, V.O. Jensen, P. Michelsen and P. Nielsen, Phys. Fluids 14, 728 (1971).
16. B.G. Christoffersen and L.P. Prahm, Plasma Phys. 14, 1140 (1972).
17. H.L. Pécseli and P.I. Petersen, Risø Report No. 290 (1973).
18. E.G. Harris, J. Nucl. Energy, Part C, Plasma Phys. 2 (1961) 138.
19. F.F. Chen, Phys. Rev. Letters 15, 381 (1965).
20. B.B. Kadomtsev, Plasma Turbulence (Academic Press 1965).
21. V. Tsytovick, An Introduction to the Theory of Plasma Turbulence.
22. This argument was suggested by Dr. N. D'Angelo.
23. K. Bol, Phys. Fluids 7, 1885 (1964).
24. N. D'Angelo and L. Enriques, Phys. Fluids 9, 2290 (1966).
25. J.R. Roth, Phys. Fluids 14, 2193 (1971).
26. C.C. Dangnney et al., Phys. Rev. Lett. 25, 497 (1970).
27. M. Keilhacker and K.H. Steuer, Phys. Rev. Lett. 26, 694 (1971).
28. C.M. Tchen, Phys. Fluids 8, 1659 (1965).
29. N. D'Angelo, H.L. Pécseli and P.I. Petersen, to be published in Phys. Fluids.

30. F.F. Chen, Phys. Fluids 9, 965 (1966).

31. S. Chandrasekhar, "Hydrodynamic and hydromagnetic stability", Oxford University Press (1961).

32. T. Obayash in "Solar-Terrestial Physics" edited by J. King and W. Newman, London (1967) p. 141.

33. D. Farley, Jr., J. Geophys. Res. 68, 6083 (1963).

34. A. Rogister and N. D'Angelo, J. Geophys. Res. 75, 3879 (1970).

35. B. Balsley, J. Geophys. Res. 74, 2333 (1969).

36. K. Bowles, B. Balsley and R. Cohen, J. Geophys. Res. 68, 2485 (1963).

37. J. Whitehead, J. Atmos. Terr. Phys. 29, 1285 (1967).

38. G. Reid, J. Geophys. Res. 73, 1627 (1968).

39. M. Schmidt and S. Gavy, J. Geophys. Res. 78, 8261 (1973).

40. R. Sudan, J. Akinrimisi and D. Farley, J. Geophys. Res. 78, 240 (1973).

41. N. D'Angelo, H. Pécseli and P. Petersen, to be published in J. Geophys. Res.

42. A. Dalgarno, in "Atomic and molecular processes", edited by D.R. Bates, Academic Press (1962).

43. D. Morse, Phys. Fluids 8, 1339 (1965).

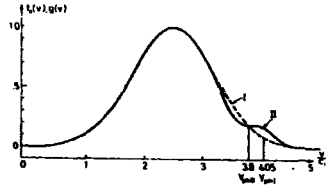


Fig. 1. Shape of the $f_0(v)$ and $g(v)$ functions.

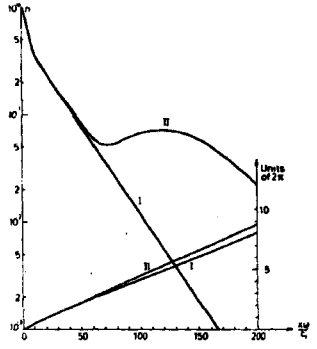


Fig. 2. Density and phase of wave calculated for the two cases.

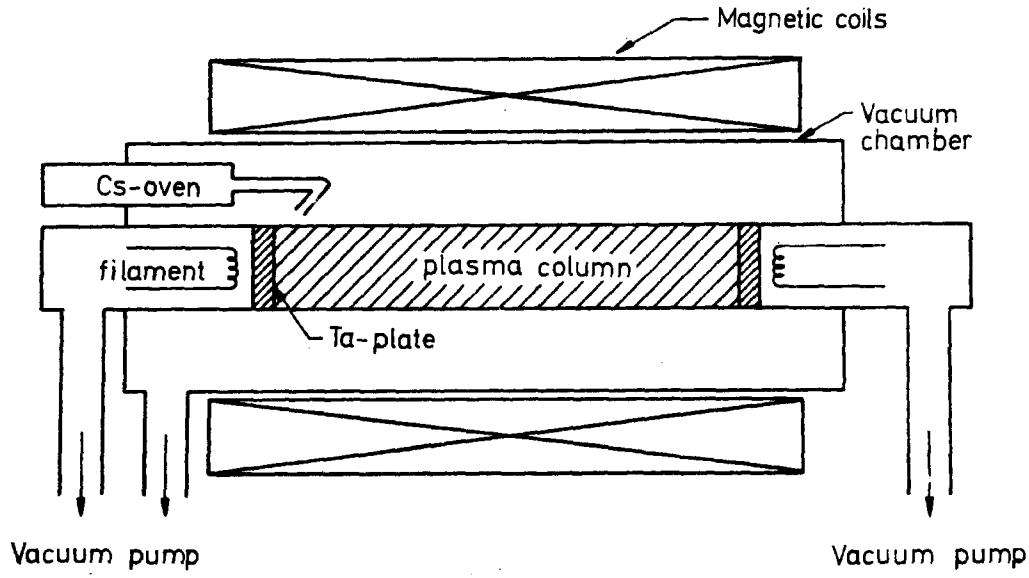
Magnetic coils
Vacuum chamber
Cs-oven
filament
plasma column
Ta-plate
Vacuum pump
Vacuum pump

FIG. 3

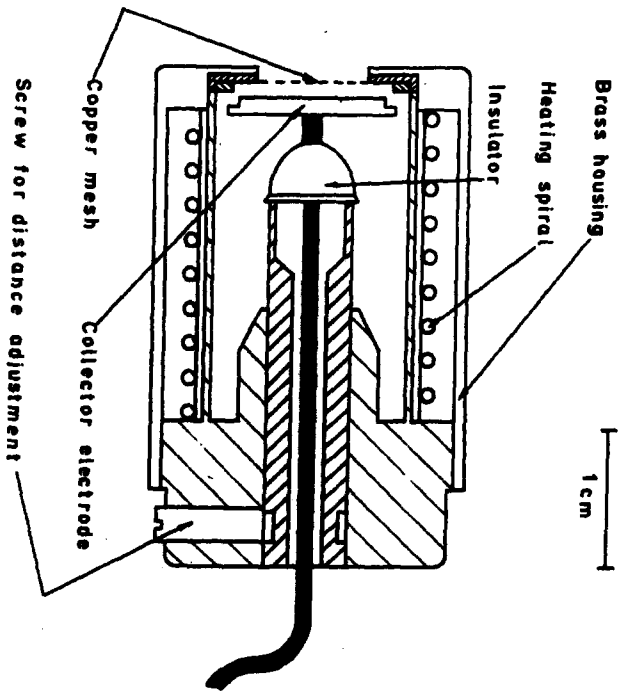
Copper mesh
Collector electrode
Screw for distance adjustment
Insulator
Heating spiral
Brass housing
1 cm

FIG. 4

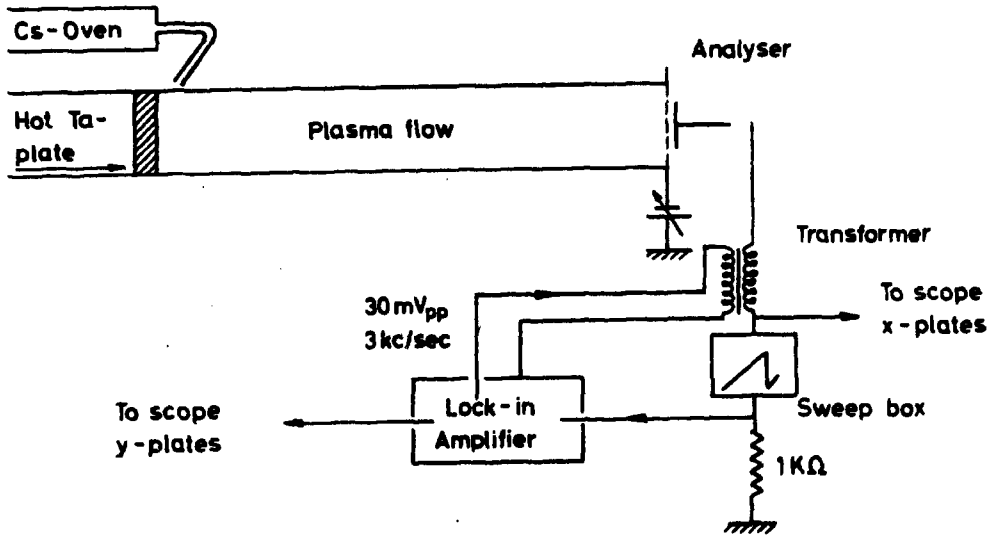
Cs-Oven
Analyser
Hot Ta-plate
Plasma flow
Transformer
30 mV$_{pp}$
3 kc/sec
To scope x-plates
To scope y-plates
Lock-in Amplifier
Sweep box
1 KΩ

FIG. 5

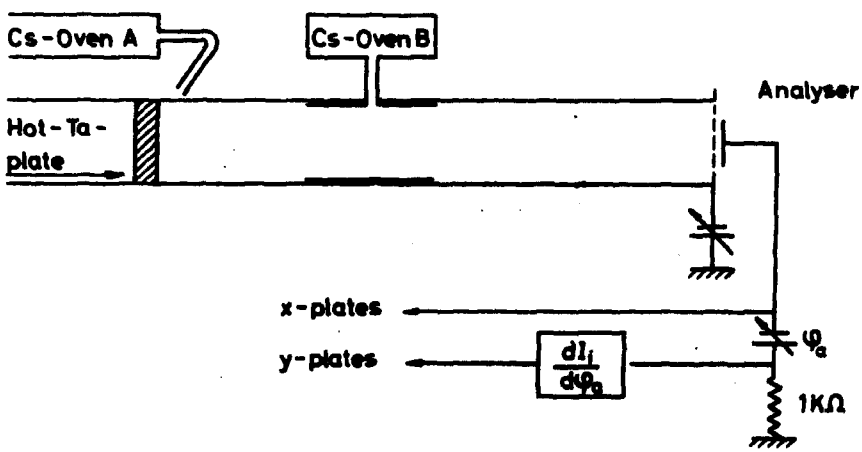
Cs-Oven A
Cs-Oven B
Analyser
Hot-Ta-plate
x-plates
y-plates
$\frac{dI_i}{d\varphi_a}$
$\varphi_a$
1 KΩ

FIG. 6

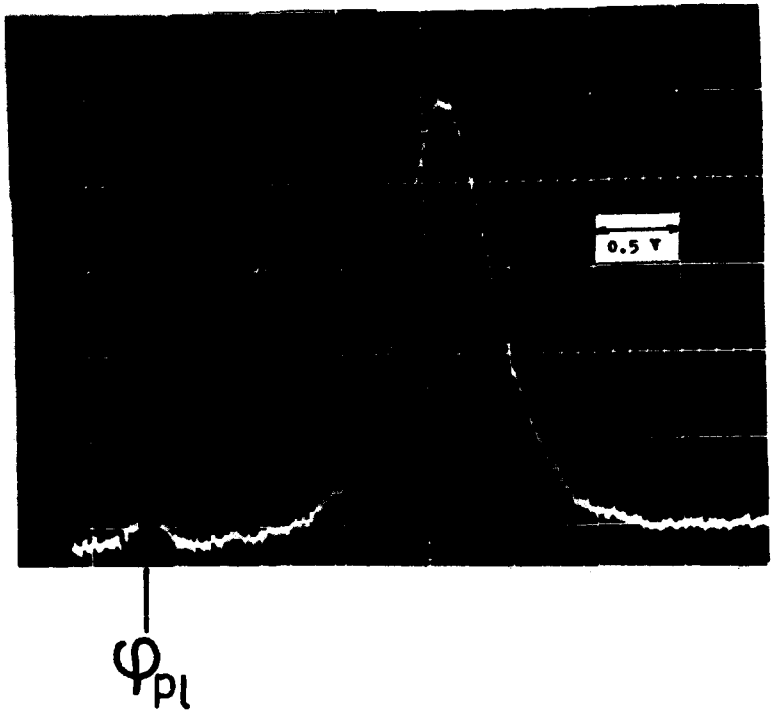


FIG.7

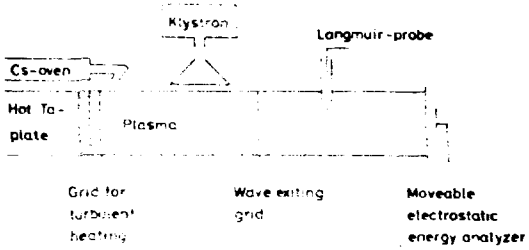


Fig. 8 [illegible] diagram of the Q-machine.

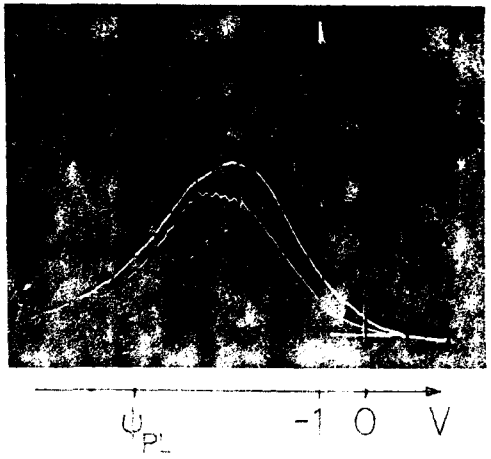


**Fig. 9.** The ion energy distribution measured with the electrostatic energy analyser. Upper trace: the electrons unheated.
Lower trace: the electrons heated by ion-[illegible] resonance.

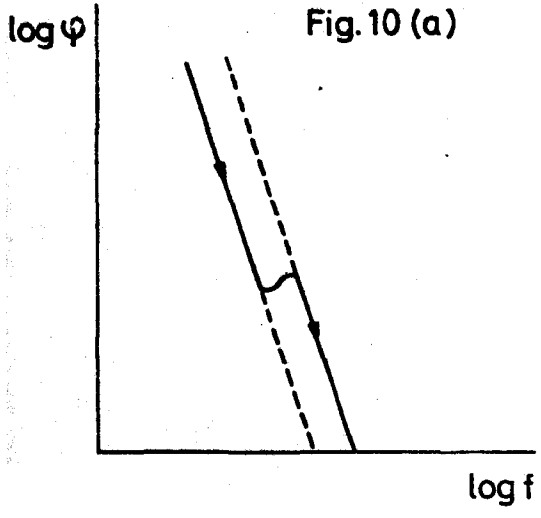


Fig. 10 (a)

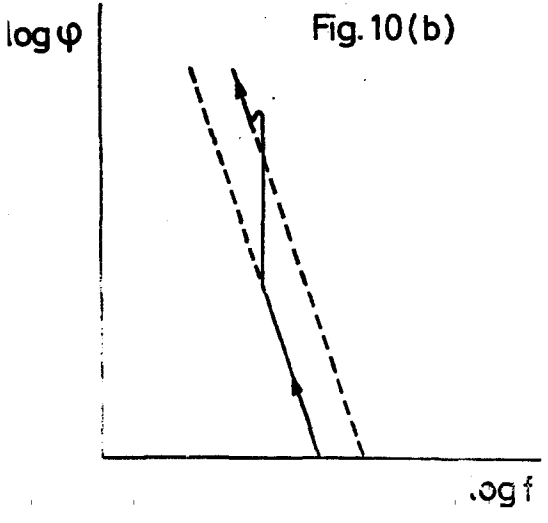


Fig. 10 (b)

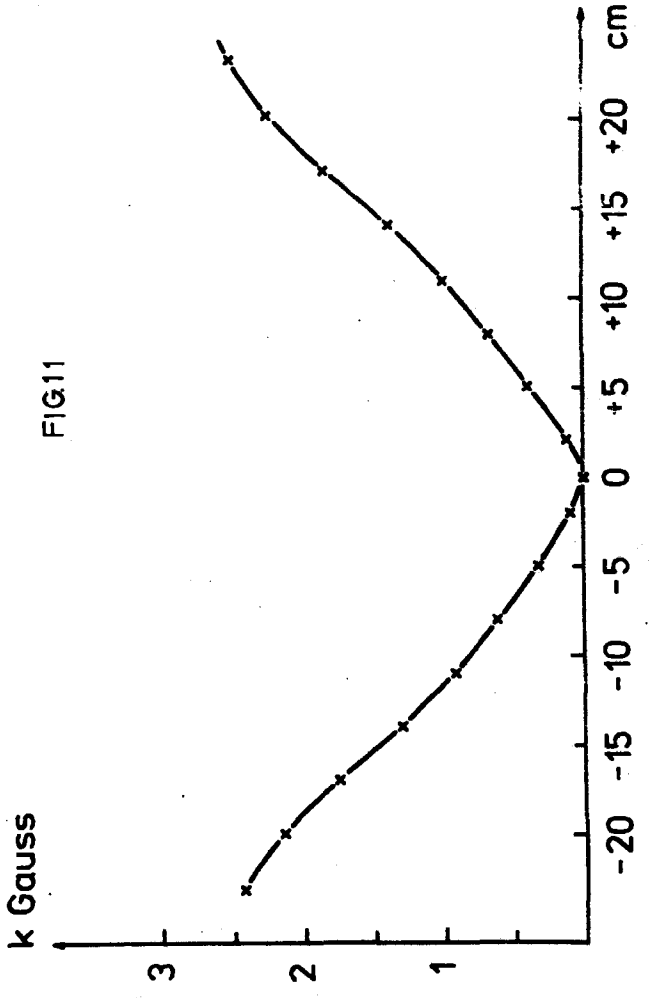


FIG11

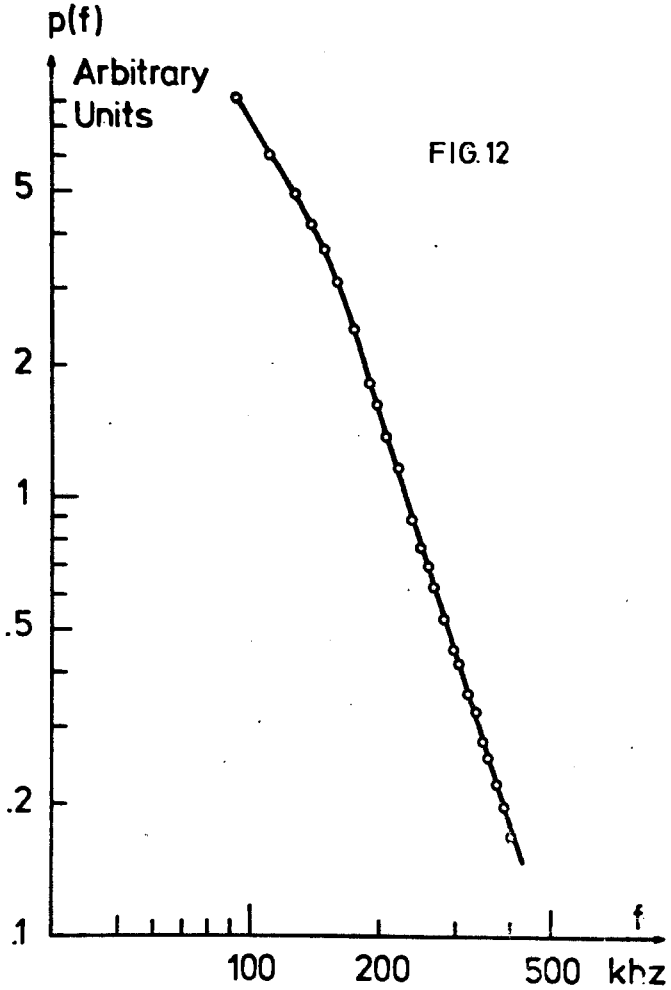
p(f)
Arbitrary
Units
5
2
1
.5
.2
.1
100
200
500
khz
f

FIG. 12

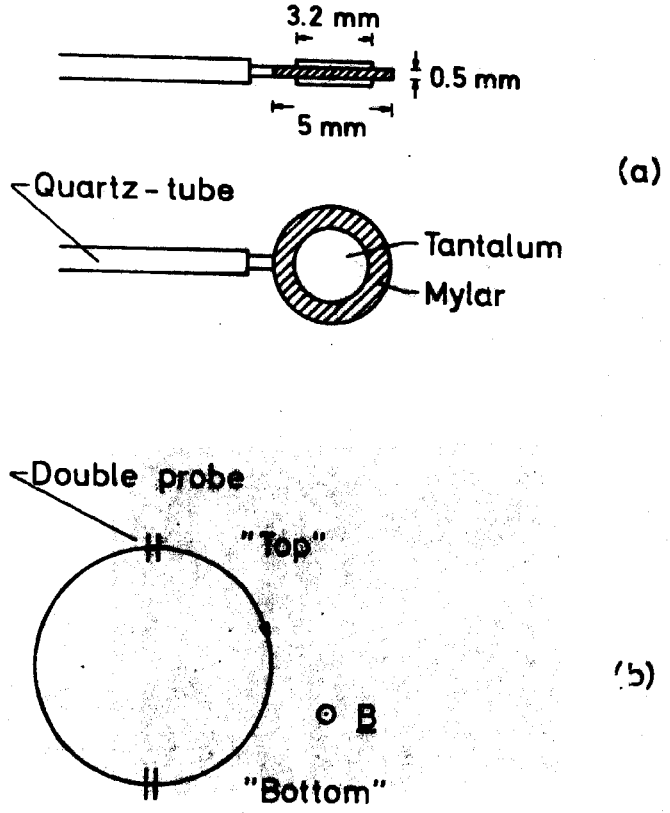
3.2 mm
0.5 mm
5 mm
(a)
Quartz - tube
Tantalum
Mylar
Double probe
"Top"
B
"Bottom"
(b)

FIG. 13

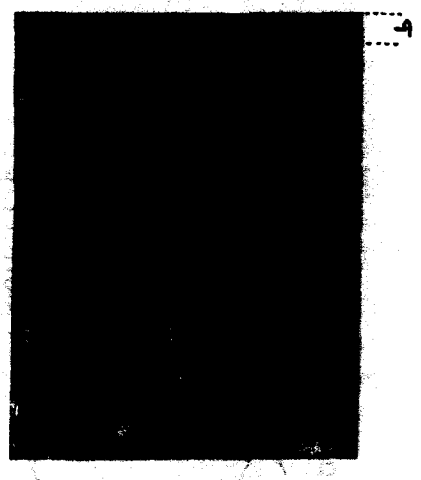

FIG. 15

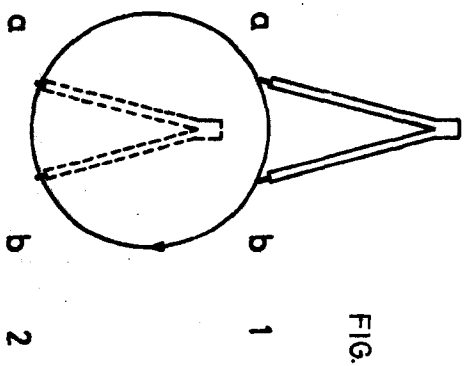


FIG. 14

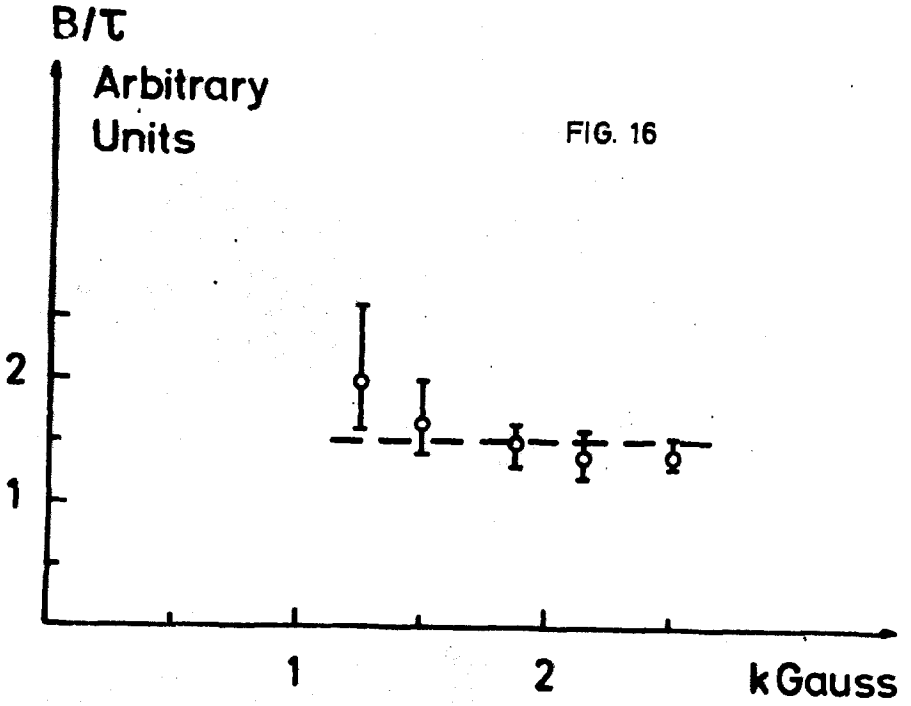


FIG. 16

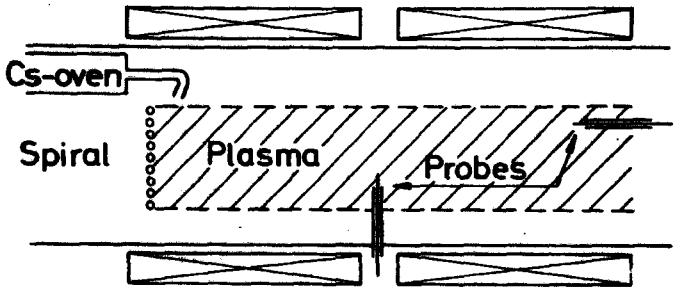


(a)

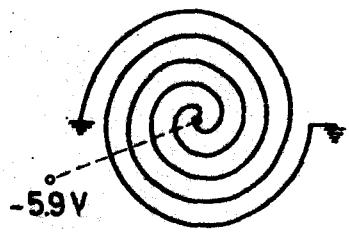


(b)

FIG. 17

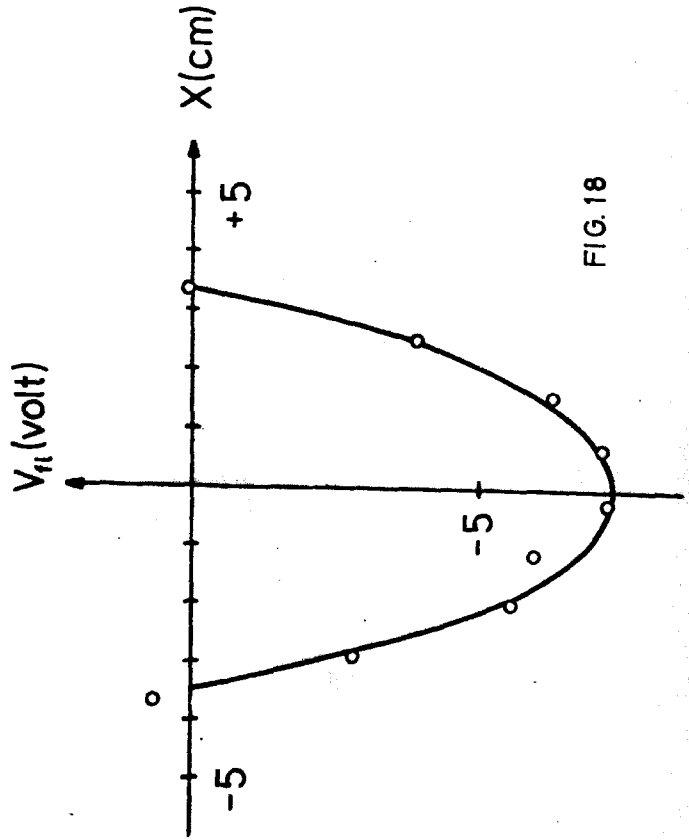


FIG. 18

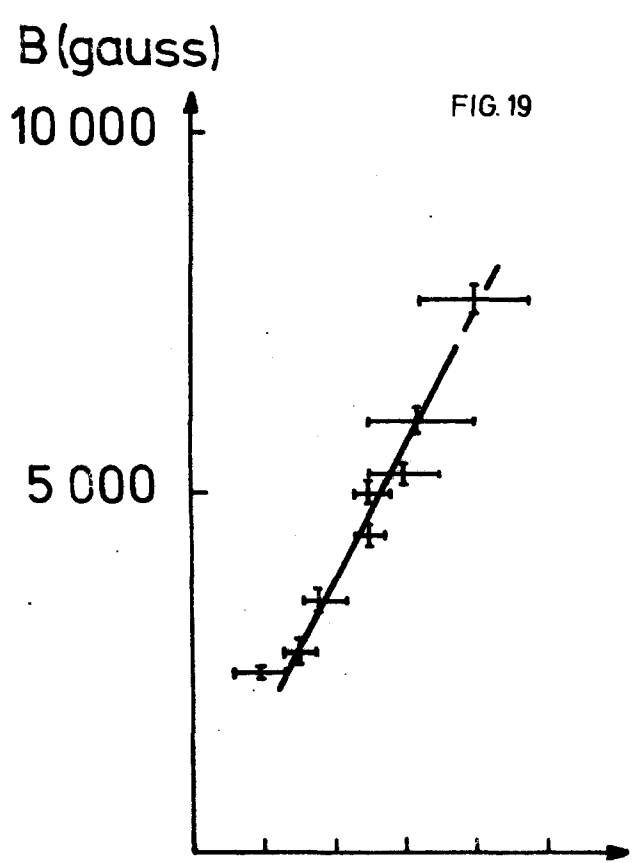


FIG. 19

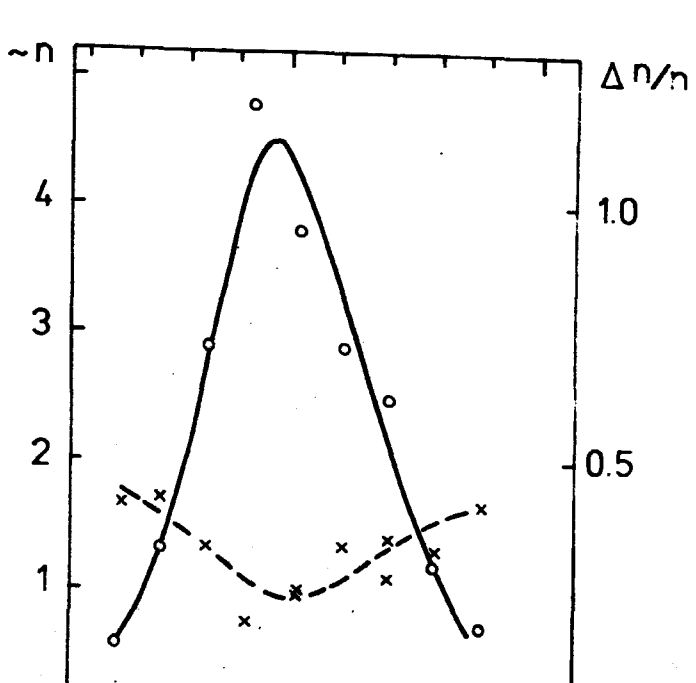


FIG. 20

1.0
0.5
$\frac{\Delta\varphi}{2\pi}$
0°
180°
360°
$\vartheta$

FIG. 21


$v \times 10^{-4}$ (cm/s)
10
5
$v_{E\times B}$
$v_{ph}$
$C_s$
5000
B (gauss)

FIG. 22

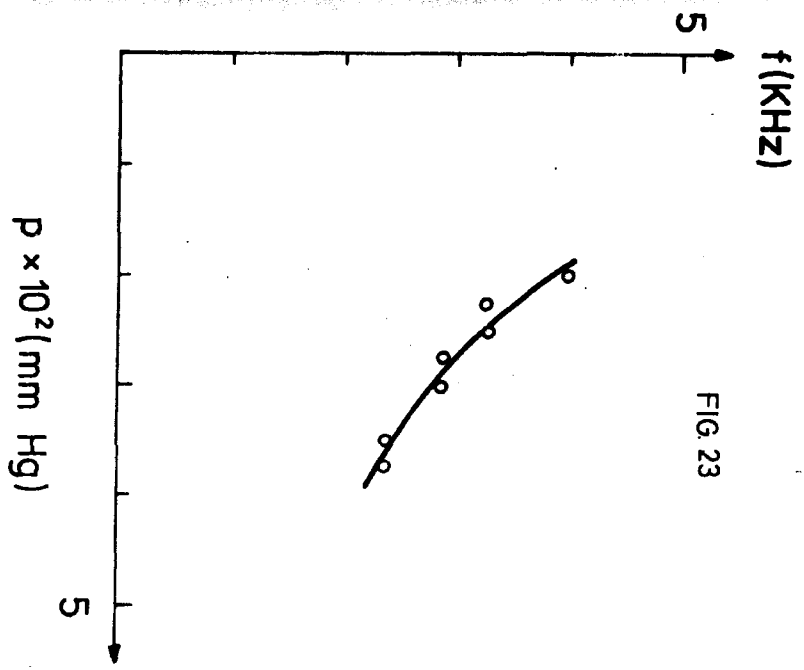
5
f(KHz)
P x 10²(mm Hg)
5

FIG. 23

Fig. 24

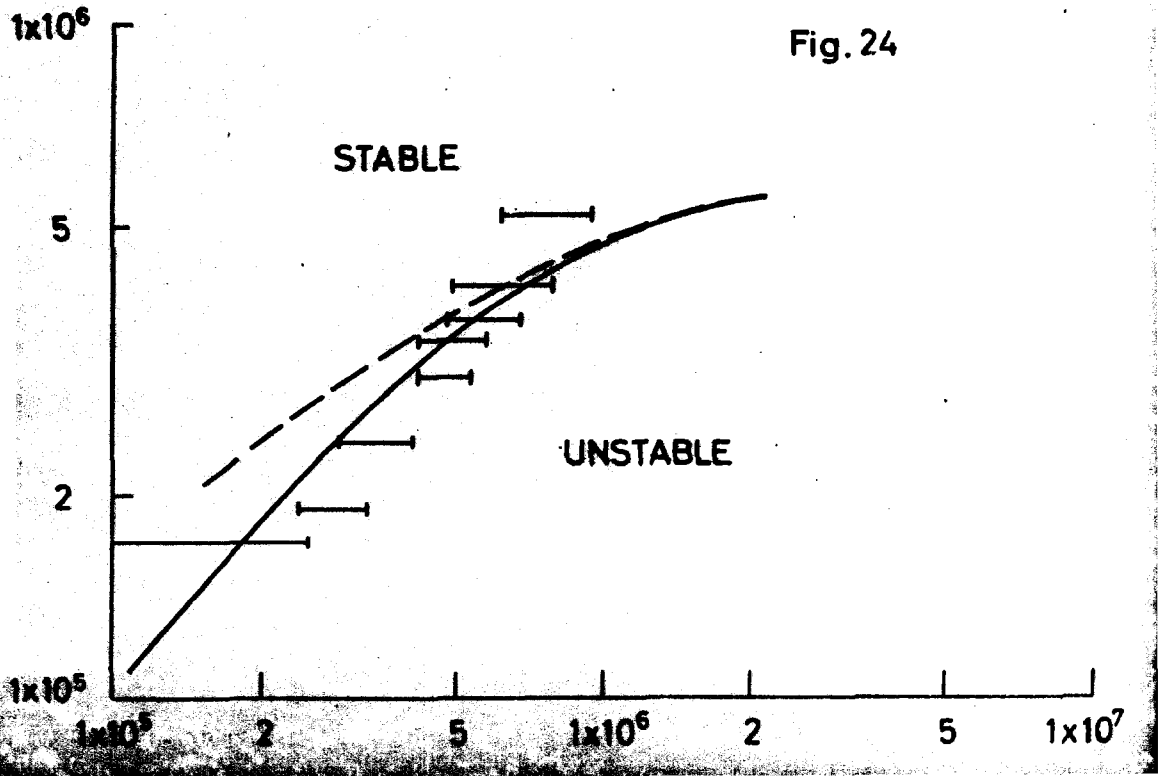
1x10⁶
STABLE
5
UNSTABLE
2
1x10⁵
1x10⁵
2
5
1x10⁶
2
5
1x10⁷